Research Paper

A novel desiccant compound for air humidification and dehumidification

Stefano De Antonellis [a], [*], Emilia Bramanti [b], Luigi Calabrese [b], [c], Beatrice Campanella [b], Angelo Freni [b]

[a] Department of Energy, Politecnico di Milano, Via Lambruschini 4, 20156 Milano, Italy
[b] CNR ICCOM - Institute of Chemistry of Organometallic Compounds, Via G. Moruzzi, 1 - 56124 Pisa, Italy
[c] Department of Engineering, University of Messina, Contrada di Dio Sant'Agata, 98166 Messina, Italy

ARTICLE INFO

ABSTRACT

Currently, there is an increasing interest in the development of HVAC systems based on solid desiccant materials to achieve efficient and affordable air dehumidification and humidification processes. Many research efforts deal with the development of novel composite materials suitable to manufacture such devices. In this work we present a novel silica gel-based desiccant compound, which can be used to prepare different products, such as sheets, monolithic components, and coatings. The proposed formulation is based on a combination of silica gel, sodium polyacrylate, vinyl glue and polypropylene fibers. The preparation procedure of the sorbent material and its characterization (adsorption capacity, morphology and surface analysis, mechanical properties by pull-off test, structural and thermal stabilities of new and aged samples and volatile compounds emissions) are described in detail. A small-scale prototype has been also manufactured and experimentally tested under typical operating conditions of air dehumidification processes. Results show that the proposed material has a suitable sorption capacity (maximum water uptake equal to 0.32 kg kg^{-1}), good mechanical properties (pull adhesion strength around 2.74 MPa) and stability (decomposition threshold of 400 °C). The performances achieved by the prototype are comparable with those of a reference silica gel packed bed system, highlighting that the desiccant material performs adequately also at system scale.

Nomenclature

A	Adsorption potential [kJ kg^{-1}]
B	Base length [m]
D	Diameter [m]
E	D-A potential [kJ kg^{-1}]
f	Mass fraction [-]
H	Height length [m]
L	Length [m]
M	Mass [kg]
n	Exponent for surface heterogeneity [-]
p	pressure
Q_{ads}	Heat of adsorption [kJ kg^{-1}]
RH	Relative Humidity [-]
T	Temperature [°C]
S	Surface/Area [m^2]
X	Humidity Ratio [kg kg^{-1}]
v	Air velocity [m s^{-1}]
W	Water content [kg kg^{-1}]

Greek Letters

ΔX	Humidity ratio variation [kg kg^{-1}]
λ	Enthalpy of evaporation of water [kJ kg^{-1}]
ρ	Density [kg m^{-3}]
τ	Half cycle time [s]

Subscripts

ads	Adsorption material
avg	Time averaged value
b	Bead
bed	Bed
d	Desiccant sheet
in	Inlet
max	Maximum
out	Outlet

[*] Corresponding author.
E-mail address: stefano.deantonellis@polimi.it (S. De Antonellis).

Note: Low-resolution images were used to create this PDF. The original images will be used in the final composition.

pro	Process
reg	Regeneration
v	Water vapor
vsat	Water vapor at saturation

Superscripts

N   Reference condition ($\rho = 1.2$ kg m^{-3})

Acronyms

D-A	Dubinin – Astakhov
DVS	Dynamic Vapor Sorption
EXP	Experimental
FT-IR	Fourier Transform - Infrared Spectroscopy
HEC	Hydroxyethyl cellulose
HS-GC	Head Space Gas Chromatography
MS	Mass Spectrometry
PVP	Polyvinylpyrrolidone
PP	Polypropylene
SEM	Scanning Electron Microscopy
SG	Silica Gel
SIM	Simulation
TGA	Thermo Gravimetric Analysis
VOC	Volatile Organic Compound

1. Introduction

Currently, there is an increasing interest in the development of HVAC systems based on solid desiccant materials to achieve efficient and affordable air dehumidification/humidification processes [1 2]. The working principle of such devices is based on the ability of some porous materials, such as silica gel and zeolites, to effectively adsorb/ desorb water vapor from/to a moist air stream. Through an appropriate design and management of the system, water vapor can be reversibly exchanged between two airflows, alternatively put in contact with the sorption material. First, a namely process air stream is dehumidified: at this stage the desiccant increases its water content until almost the saturation is reached. Then, a second air stream, conventionally indicated as regeneration one, is heated by an external source (even at low temperature, such as 40–50 °C) and used to remove water vapor from the sorption material. Since air dehumidification occurs at the process side and air humidification at the regeneration one, the device can be effectively designed to provide humidity ratio variation of an airflow. An exhaustive overview of such devices and related applications is reported in [3].

Silica gels and common silicoaluminate zeolites (such as 13X and 4A) are the most commonly adsorption materials employed in solid desiccant heat and mass exchangers, mainly due to their large availability on the market and relatively high affinity with water molecules (sorption capacity up to 0.4 kg kg^{-1}) [45]. On the other hand, silica gel is an amorphous material with intrinsically poor hydrothermal and mechanical stabilities, while silicoaluminate zeolites require high regeneration temperature (beyond 150 °C) at low p_v/p_{vsat} ratio. In addition, sorption materials are generally available in the form of powders, granules or beads: for both powder and granules, the process necessary to coat surfaces or to manufacture monolithic components or sheets is very complex; for beads, the spherical or cylindrical geometry limits the design of the device.

In recent years, many research efforts dealing with sorption materials, substrates, and binders, have been carried out to overcome such limitations. New types of solid desiccants have been suggested, including crystalline (silico)aluminophosphate (such as AlPOs and SAPOs) [6

7], metal–organic frameworks (MOFs) [8 9] and composite adsorbents, constituted by a salt inside silica or carbon porous host matrix [10 11 12]. In general, such advanced materials can guarantee outstanding water adsorption capacity (up to 0.8 kg kg^{-1}), which allows the design of compact solid desiccant units. However, many materials have been developed only at laboratory level or are highly expensive, which is a bottleneck for their practical utilization in actual devices [13 14].

Recent R&D efforts have been focused on the optimal integration between the supporting substrate and the adsorbent material through the development of coated desiccant heat exchangers. This approach can offer better heat and mass transfer properties as well as higher dehumidification and humidification capacity of the airflow, with respect to conventional packed stationary beds or rotary wheels [15 16]. Two different approaches are currently under investigation: the direct synthesis of the adsorbent material over the substrate surface and binder-based dip / spray coating technique [17].

The direct synthesis method consists in the grown of a thin layer (10–50 μm) of zeolite crystals on the surface of a large surface area heat exchanger by hydrothermal deposition process [18 19]. This method provides a good interaction between the adsorbent layer and the substrate, increasing the heat exchange efficiency. However, the severe synthesis conditions, especially for SAPO zeolites, and the low material thickness (10–50 m), limit the practical industrialization of this technique [20]. Moreover, the dense structure of the adsorbent layer can significantly limit the internal vapor diffusion. The mass transfer issue has been partially solved by using macro porous structures, such as metal or carbon-based foamed zeolite [21 22] or a metal fibers network [23], which allow to maintain good heat exchange and offer high mechanical stability without affecting vapor diffusion through the desiccant material.

Alternatively, relevant research activities have been focused to develop coated adsorbent heat exchangers by spray or dip-coating technique. In this case, the coating preparation procedure involves the addition of a certain amount of polymeric binder: adsorbent layers with 0.1–0.3 mm thickness are typically achieved [24 25]. Polyvinyl alcohol, polyvinyl pyrrolidone, epoxy resins, silanes and silicones are commonly used binders [26 27 28 29 30], which allow to increase the adsorbent layer thermal conductivity and to maintain sufficiently high permeability to vapor diffusion through the adsorbent layer [31]. Furthermore, coating process based on silica gel and polymeric binder can be easily scaled up at industrial level and are sufficiently affordable, being silica gel cheap and largely available on the market. Based on the aforementioned considerations, in Tab. 1 recent research works about silica gel – polymer compounds are summarized, reporting main performed characterizations, performance results and available thermophysical data.

However, looking at the previous state of art, still some research gaps need to be addressed. In particular, the presence of an organic binder in the coating formulation could potentially yield the partial blockage of pores and the production of volatile organic compounds due to thermal ageing. Additionally, low mechanical strength and poor hydrothermal stability are possible issues that should be properly addressed to meet durability requirements of commercial products [37].

The design of an adsorbent compound, cheap and easily made, which has an effective adsorption/desorption capacity and able to preserve a suitable mechanical stability during the hydrothermal cycles, is a relevant aspect that should increase the scientific soundness of this research topic. (See Table 1).

To overcome the above-mentioned problems, in this work we present a novel silica gel-based desiccant compound, which can be used to prepare different products, such as desiccant sheets, monolithic components and coatings. The high manufacturing flexibility is an added value able to address its use in different application contexts, allowing to tailor the performance and geometry of the adsorbent product according to the industrial constrains. The novel compound formulation

Table 1

Recent research works on silica gel – polymer compounds.

Adsorbent	Binder type and amount	Configuration	Performed characterizations	Max water uptake	Main results
Microporous silica gel (Fuji Silysia Chemical Ltd, Japan) [32]	PVP (2 wt%)	Consolidated disks; f = 17 mm; thickness = 1.1–1.5 mm	Porous structure by N_2 physisorption; Adsorption isotherms; Thermal diffusivity and conductivity;	W = 0.3 kg kg^{-1} (T = 30 °C, p = 4 kPa)	Packing density = 834–975 kg m^{-3}; Average sorption enthalpy = 2580 kJ kg^{-1}; Thermal conductivity = 0.16 W m^{-1} K^{-1}
Mesoporous silica gel (SiliaFlash, Silicycle, Canada) + CaCl2 (28 wt%) [33]	PVP (10 wt%) + graphite flakes (20 wt%)	Consolidated disks; thickness = 3.5 mm;	Porous structure by N_2 physisorption; Adsorption isotherms; repeated sorption cycles; Thermal diffusivity and conductivity;	W = 0.2 kg kg^{-1} (T = 35 °C, p = 1.1 kPa)	Thermal conductivity = 0.27 W m^{-1} K^{-1}; ethanol as solvent
Microporous silica gel, (Fuji Silysia Chemical Ltd, Japan) [34]	HEC (n.a.)	Dip-coating; average thickness = 0.1 mm;	Adsorption isotherms; Adsorber testing	W = 0.4 kg kg^{-1} (RH = 80%-90%)	Moisture removal capacity 7.4–11 g kg^{-1} (air flow rate = 35 kg h^{-1})
Microporous silica gel, (Fuji Silysia Chemical Ltd, Japan) [35]	liquid glue (10 wt%)	Coating sheets; 100 mm × 20 mm; thickness = 0.05–0.38 mm;	Adsorption isotherms; Sorption kinetics	W = 0.24 kg kg^{-1} (T = 30 °C, RH = 90%)	Coating density 523–888 kg m^{-3}; Thermal conductivity = 0.11 W m^{-1} K^{-1};
Microporous silica gel type [28]	HEC (3.3 wt%)	Dip-coating; average thickness = 0.7 mm;	Adsorption isotherms; Adsorber testing	W = 0.42 kg kg^{-1} (T = 35 °C, RH = 90%)	High heat and mass transfer (1.5–2 times faster than conventional granular configuration)
Silica gel + LiCl (30 wt%) [36]	Emulsion binder (~15 wt%)	Coating sheets; 120 mm × 80 mm; thickness = 0.3 mm;	Adsorption isotherms; Adsorber testing	W = 0.25 kg kg^{-1} (T = 30 °C, RH = 90%)	Binder thermal conductivity = 0.24 W m^{-1} K^{-1}
Mesoporous Silica gel (Shanghai Ling Yi Gong Mao Co. China) + LiCl (16.12 wt%) [10]	Liquid glue (n.a.)	Coating sheets thickness n.a.	Porous structure by N_2 physisorption; Adsorption isotherms; Thermal diffusivity and conductivity, Sorption kinetics	W = 0.65 kg kg^{-1} (T = 20 °C, RH = 90%)	Dehumidification capacities > 25–45% when compared to silica gel

is based on a proper combination of sodium polyacrylate and vinyl glue as binders, based on the previously reported stability and good affinity with adsorbent materials [38 39], and polypropylene fibers, to further improve the adsorbent layer mechanical strength. The preparation procedure of the material is described in detail. The morphology and surface analysis of the desiccant sheets have been evaluated by Scanning Electron Microscopy (SEM). Mechanical properties of the composite material realized have been evaluated by pull-off test. Adsorption, structural and thermal stabilities of new and on-purpose aged samples have been investigated respectively by sorption isotherms measurement, Thermo-gravimetric (TG) test and Fourier Transform - Infrared Spectroscopy (FT-IR) analysis. Evaluation of the presence of undesired volatile compounds has been carried out by Head Space Gas Chromatography / Mass Spectroscopy (HS-GC/MS) technique. Finally, a small-scale prototype has been manufactured and experimentally tested under typical operating conditions of an air dehumidification process. Performances achieved by the proposed prototype are compared with those of a reference silica gel packed bed system.

2. Experimental part

2.1. Sample preparation

The components used for the preparation of the adsorbent material are listed below:

1. Commercial Silica Gel in powder state, produced by Silysiamont. According to manufacturer data, average particle diameter is 7 μm, average pore size is 2.5 nm, pore volume is 0.4 ml g^{-1}, specific surface area is 700 m^2 g^{-1} and sorption capacity, at 50 °C, is around 0.2 and 0.55 kg kg^{-1} respectively at RH equal to 40% and 90% (further sorption properties are discussed in section 3.2).
2. Sodium polyacrylate distributed by Alquera SL.
3. Commercial vinyl glue.
4. Demineralized Water.
5. Polypropylene fibers (0.6 mm length).

The basic composite material (slurry) was prepared by mixing the components according to mass fraction detailed in Table 2. The quantity of each component was optimized to get a material with adequate mechanical properties and to minimize the amount of binder. Preliminarily, sodium polyacrylate, vinyl glue and water were mixed until a homogeneous solution is reached. Afterward, silica gel filler and polypropylene fibers were progressively added in a small container, at room temperature (around 20 °C). The slurry was manually stirred for ten minutes up to homogeneity and, subsequently, it was placed and kept in a closed vessel for 30 min before following product preparation.

The mixture can be used to prepare different products, such as desiccant sheets, monolithic components, and coatings. Fig. 1 schematizes the preparation steps applied for the silica gel filled composite material.

2.1.1. Sheet

A small layer of material (e.g. 2 mm) was spread evenly on a non-stick polypropylene board. The panel was then placed in oven at 45 °C and held until the material was dry (about 4 h). Finally, the oven temperature was raised up to 75 °C and the material was kept at 75 °C for one hour, until it spontaneously detached from the surface of the panel. Fig. 2A shows an example of the final product.

2.1.2. Monolithic structure

The slurry was placed inside a Teflon mold and heated in an oven at 75 °C. Differently to sheets, due to larger thickness of monolithic struc-

Table 2

Mass fraction and density of slurry materials.

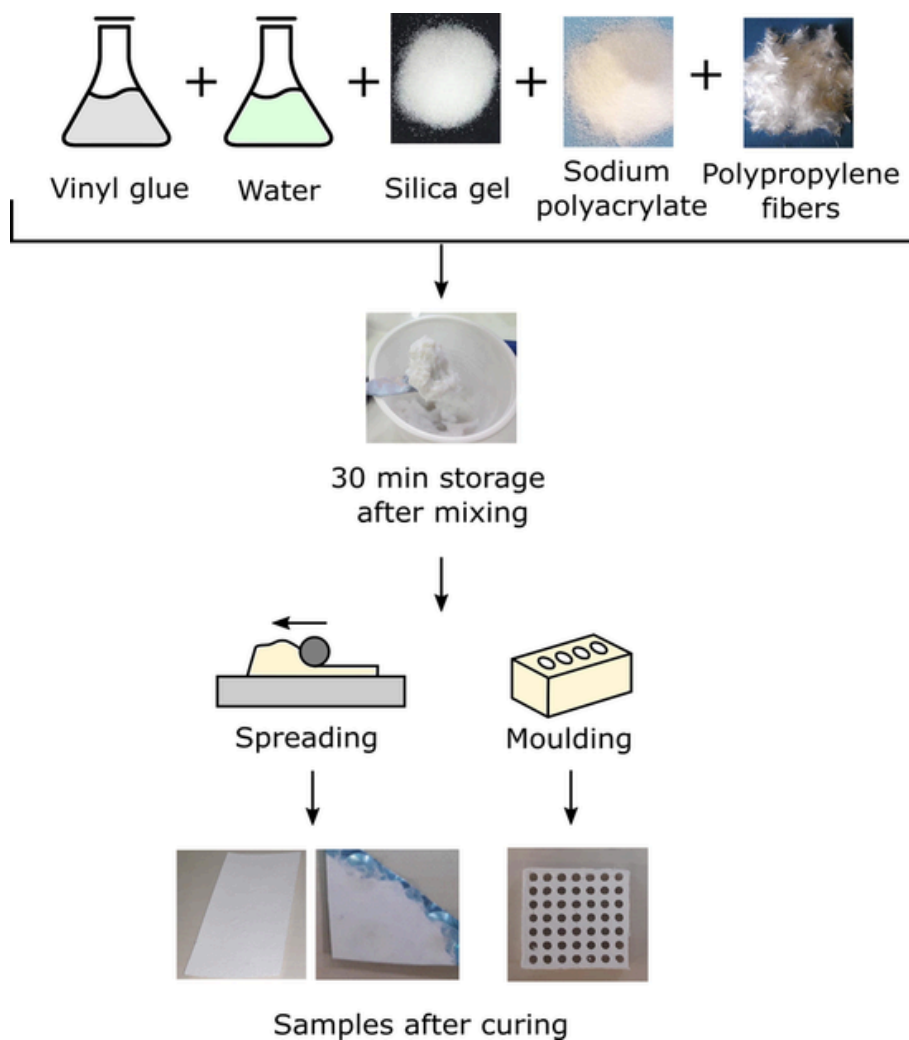| Material	Mass Fraction	Density
Silica Gel	17.5%	0.70 g ml^{-1}
Sodium Polyacrylate	1.1%	1.22 g ml^{-1}
Vinyl Glue	35.5%	1.19 g ml^{-1}
Distilled Water	45.2%	1.00 g ml^{-1}
PP Fibers	0.7%	0.90 g ml^{-1}
Total	100.0%	

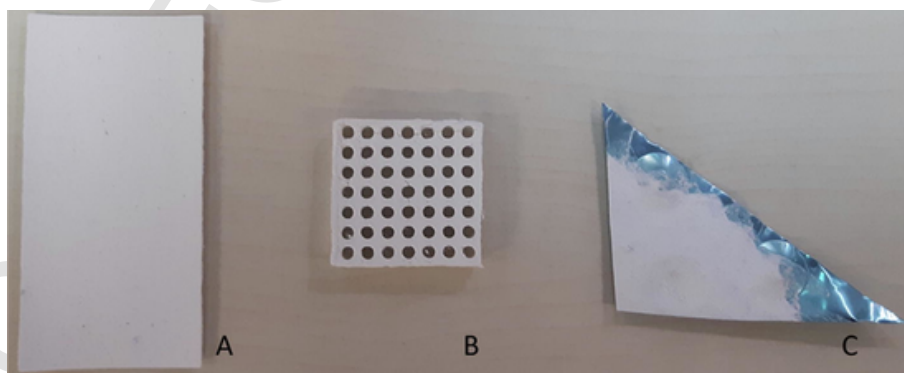**Fig. 1.** Preparation scheme of the silica gel composite material.

Fig. 2. Sample typology: A) Desiccant sheet; B) Monolithic structure; C) Coating on hydrophilic aluminum.

ture, a longer drying time was required. A completely dry material was obtained after 12–24 h, depending on the thickness (range 0.5–1.5 mm) of the monolithic structure. At the end of the process, the external and internal parts of the mold were removed to extract the monolithic structure with the desired characteristics. In Figure 2B, a small complex structure (5.5 cm length, 5.5 cm width, 1.0 cm height) with several circular holes inside is shown. The sample preserved the shape of the mold even after the shrinkage that occurred during the drying phase. The specimen is regular and without macroscopic heterogeneities.

2.1.3. Coating

The composite slurry was also successfully employed to produce surface coatings, after dilution with additional water (approximately 0.3 parts of additional water for each part of the composite slurry). In the example shown in Fig. 2C, an aluminum sheet was coated using the brush-applied diluted slurry (several layer can be applied until the desired thickness is reached), after a hydrophilic treatment was applied on the surface to increase the adhesion of the coating with the substrate. Finally, the sample is heated in an oven at 75 °C until completely dried.

2.1.4. Conclusion on sample preparation

According to aforementioned preparations, after the completion of the oven drying process, the slurry weight decreases significantly due to the evaporation of water and solvents. The mass ratio between dry sample and initial slurry was 0.24 (indicating a weight reduction of about 76%). The mass fraction of silica gel f_{SG} in dry sample (mass of silica gel to mass of dry sample) was equal to 0.73.

2.2. Adsorption, morphological and mechanical analysis

To assess the structural stability of the composite adsorbent material, morphological and mechanical analysis of sample in the sheet form (as described in section 2.1.1) were carried out. In particular, optical microscopy was performed by using a three-dimensional digital microscope (Hirox HK-8700) and surface morphology was evaluated by an environmental scanning electron microscopy (ESEM, Quanta 450, FEI, Hillsboro, OR, USA).

Furthermore, pull-off adhesion tests (by using a DeFelsko PosiTest AT-M pull-off tester) were performed, according to ASTM D4541 standard, to assess the adhesion strength of the composite coating on an aluminum sheet substrate. According to the experimental procedure reported in [40], an aluminum dolly (10 mm diameter) was glued on the coated surface using a commercial epoxy compound. Afterward, all samples were cured at room temperature and open to air for 24 h before carrying out the tests. Three replicas for each sample were performed.

Water adsorption isotherms were measured through a gravimetric adsorption apparatus (Aquadyne DVS analyzer). Tests were performed at three different temperatures: 30 °C, 50 °C and 70 °C. The reference state of the material (anhydrous condition) was obtained in nitrogen atmosphere at 80 °C (atmospheric pressure). Experimental uncertainty of measured quantities are the following: temperature - ± 0.2 °C; relative humidity - from ± 0.8% at 20 °C to ± 1.8% at 70 °C; weight - ± 1.0 μg plus 0.001% of suspended mass.

2.3. Stability analysis

2.3.1. Adsorption/desorption stability

The sorption, structural and thermal stability was investigated by ageing a sample of a desiccant sheet (Fig. 2A). Two different ageing processes, namely test 1 and 2, have been implemented, both performed through the DVS equipment:

1. One hundred adsorption/desorption cycles at constant temperature and different relative humidity, based on the following steps:
   - 30 min at $T = 45$ °C and $RH = 80$ %.
   - 30 min at $T = 45$ °C and $RH = 5$ %.
2. One hundred adsorption/desorption cycles at variable temperature and relative humidity, in the following way:
   - 60 min at $T = 60$ °C and $RH = 5$ %.
   - 60 min at $T = 30$ °C and $RH = 60$ %.

Although in actual components the regeneration is obtained through temperature swing, in the ageing tests described above, the temperature was kept constant (test 1) or varied in a quite long time (test 2). In fact, due to the high thermal capacity of the adopted equipment (DVS), it was not possible to reproduce a fast adsorption/desorption cycle through an appropriate variation of the chamber temperature. Finally, it is highlighted that two different samples have been used in test 1 and 2.

To assess the structural stability of the composite material, FT-IR analyses were performed before and after the ageing process. Infrared spectra were recorded by using a Perkin-Elmer Frontiers FT-IR Spectrophotometer, equipped with a universal attenuated total reflectance (ATR) accessory and a triglycine sulfate TGS detector. For each sample

32 scans were recorded, averaged and Fourier-transformed to produce a spectrum with a nominal resolution of 4 cm^{-1}.

2.3.2. Thermal stability

Comparative thermo-gravimetric analysis (TGA) was performed to assess the thermal stability and estimate the degradation temperatures of the desiccant sheet. TG analysis was carried out using a Seiko EXSTAR 7200 TGA/DTA instrument. Measurements were carried out under nitrogen flow (200 ml/min) in the 30–800 °C range, at heating rate of 10 °C/min scanning rate, on 5–10 mg samples. The analysis of the thermograms was used to determine the temperature values corresponding to the onset, different weight loss percentages and maximum degradation for each degradation step (from DTG curves) and the final residue at 800 °C.

Furthermore, headspace-gas chromatography/mass spectrometry (HS-GC/MS) analysis was carried out to determine the compounds that possible degrades at low temperature in the composite materials. An Agilent 6850 gas chromatograph, equipped with a split/splitless injector, was used in combination with an Agilent 5975c mass spectrometer. A CTC CombiPAL auto-sampler was employed for HS sampling. Vials with 1 g of sample were incubated at 80 °C for 15 min. A 0.5 ml headspace volume was then sampled (gas-tight syringe held at 85 °C) and injected in the gas chromatograph. The syringe was then flushed with helium. The inlet liner (internal diameter of 1 mm) was held at 200 °C and the injection was performed in splitless mode. Compounds were separated on a polar column (DB-WAX ultra inert; length: 30 m; stationary phase: bonded polyethylene glycol; 0.25 mm inner diameter; 0.50 μm coating) using the following temperature program: 10 min at 30 °C, then 5 °C/min to 60 °C (held for 2 min) followed by 10 °C/min to 240 °C (held for 9 min). The temperature of the transfer line was set at 250 °C. After GC separation, compounds were ionized in positive EI, and the acquisition was performed in full scan mode. Spectral identification was done when the spectra and the NIST spectral mass library (NIST 05) combined with our in-house library matched with a spectral similarity > 90%. The thermal treatment and the analysis were repeated for three times on the same sample. Afterwards, samples were analyzed before and after thermal annealing at 80 °C for 8 h under vacuum. In this case, for HS analysis vials with 1 g of sample were incubated at 50 °C for 15 min.

3. Results and discussion

3.1. Morphological and mechanical analysis

Fig. 3 shows the top view and fractured section micrographs at 300x magnification, respectively, of the silica gel based composite sheet. The material structure is homogeneous and almost compact. No evidence of large cracks or voids can be highlighted. The morphology (Fig. 3A) is quite rough, with some asperities randomly distributed on the surface. This morphology is almost common in composite polymer adsorbent coatings and binder based composite coating and it is not strictly associated to a poor distribution of matrix binder or local filler domains [41]. Moreover, the silica gel grains are homogeneously distributed and well packed in the polymer matrix confirming a suitable interaction between the filler and the polymer matrix. It is also clear the presence of the polypropylene reinforcing fibers well embedded in the matrix. Some pores or rivers are superficially observed: these are attributable to the evaporation process of liquid solvents during the drying phase. Although, these surface asperities are not deep enough to prejudice the structural integrity of the material bulk. In fact, by analyzing the cross section of the sample (Fig. 3B) it is possible to highlight that no relevant heterogeneities or voids can be identified in the bulk of the absorbent sheet. On the fracture surface, it is possible to observe some polypropylene fibers pulled out from the matrix due to the tensile stress applied during the local ripping of the adsorbent
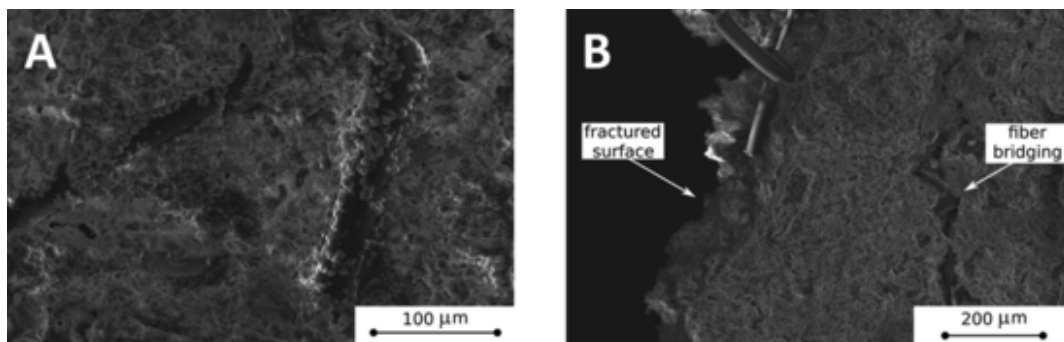
Fig. 3. Top view a) and fracture section b) micrographs of the silica gel polymer composite.

sheet. The fracture image also evidences the bridging effect offered by the polymer fiber on the crack stabilization. The reinforcement hinders the extension of the crack by imposing higher stress values to propagate the fracture of the sample. Thus, the fibers act as reinforcement allowing to anchor and to fix the constituents each other, increasing the mechanical stability of the sheet even in the presence of local cracks or fractures.

Fig. 4 shows a representative fracture surface caused of pull-off adhesion test and suggests further observations. All replicas exhibited an almost similar fracture surfaces with mainly pull-off cohesive fracture. This behavior can be related to the triggering and propagation of cracks within the bulk of the material. This indicates that the adhesion strength with aluminum substrate is stronger than the cohesive bulk one. The substrate roughness can improve both chemical and physical interaction with the applied coating, thus improving the adhesive force at the coating/substrate interface and favoring a cohesive mode failure [42]. The average pull adhesion strength is equal to 2.74 ± 0.73 MPa. This value is compatible with the literature data [37] and suggests that the composite material exhibits good tensile adhesion capability.

3.2. Adsorption properties analysis

Fig. 5 shows experimental equilibrium data of pure silica gel and of the composite material ($T = 50$ °C). The sorption capacity is calculated referring both to the total mass of the sample and to the sole mass of the silica gel (both in anhydrous conditions). The shape of all curves is similar, highlighting that their sorption capacity is substantially related to silica gel physical properties, and the amount of sodium polyacrylate is small so that it does not modify indeed the shape/slope. As expected, the sorption capacity of the material is limited due to the presence of the binder. By comparing the trend of the sorption capacity of the material with that of pure silica gel, we can state that about 60% of the adsorbent properly works, while pores of the remaining part are not available due to the presence of the binder.

Fig. 4. A representative pull-off fracture image of the composite material coated on aluminum substrate. Other replicates show the same features.
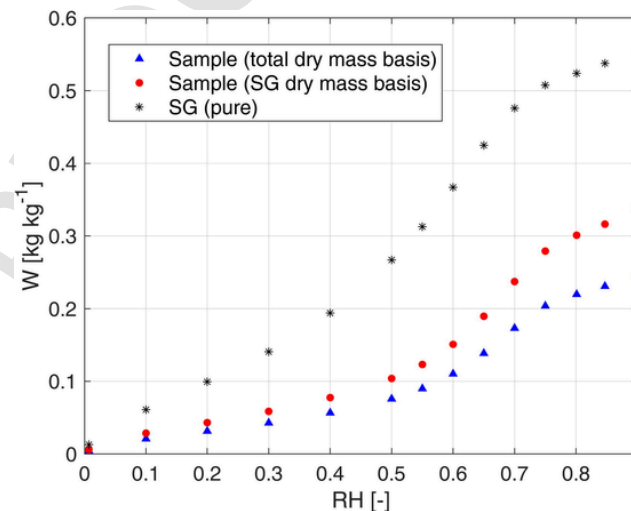

Fig. 5. Adsorption capacity at 50 °C vs relative humidity of pure silica gel (SG) and of the material developed in this work (referred to total dry mass and to dry silica gel mass).

The adsorption capacity of the composite adsorbent can be evaluated through the Dubinin-Astakhov (D-A) approach:

$$W = W_{max} e^{-\left(\frac{A}{E}\right)^n} = W_{max} e^{-\left(\frac{RT\ln(1/RH)}{E}\right)^n} \qquad (1)$$

Where W_{max} is the maximum water content, A and E respectively the adsorption and D-A potential and n the exponent for surface heterogeneity. Experimental data at 30 °C, 50 °C and 70 °C have been used to determine the parameters of Eq. (1) (on total dry mass basis): resulting values are $W_{max} = 0.3129$ kg kg^{-1}, $E = 36.47$ kJ kg^{-1} and $n = 0.9897$ ($R^2 = 0.97$). Measured data and numerical results are reported in Fig. 6.

According to D-A approach used to evaluate the adsorption capacity of the compound, the heat of adsorption can be simply calculated as follows [43]:

$$Q_{ads} = \lambda + A \qquad (2)$$

As shown in Fig. 7, Q_{ads} is close to the enthalpy of evaporation at a given temperature: at low water content Q_{ads} is around 10% higher than λ while at maximum sorption capacity Q_{ads} tends to λ.
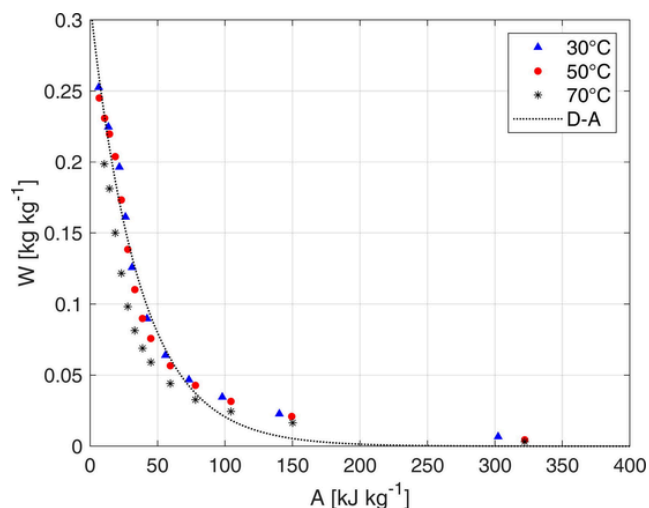
Fig. 6. Measured and calculated adsorption capacity of the new material (numerical results obtained with Dubinin-Astakhov Eq. (1)). Values are calculated on total dry mass basis.
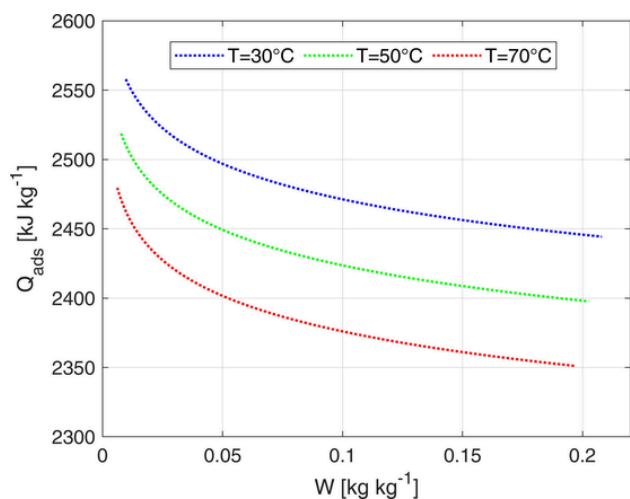

Fig. 7. Calculated heat of adsorption of compound (Eq. (2)).

3.3. Verification of stability

3.3.1. Adsorption/desorption stability

The adsorption and desorption capacity were observed during the ageing process carried out through the DVS apparatus. Fig. 8 shows last 10 cycles of the two stability tests (denoted as 1 and 2 and described in Section 2.3.1): no evidence of performance degradation is shown, since the maximum and minimum water uptakes do not change even after several adsorption/desorption ageing cycles.

The ascending and descending branch of *W* is almost similar. This qualitatively suggests that the kinetic diffusion of water vapor through the composite bulk is not hindered up to 100 cycles of test 1 and test 2.

With the purpose of assessing the structural stability of the composite material and their constituents, FT-IR analyses were performed on aged and unaged samples (before and after the 100 cycles of test 1). The results confirmed the presence of each single component employed for the preparation of the material (silica, polypropylene fibers, polyacrylate, vinyl binder), as shown in Fig. 9A. The band at 3600–3000 cm^{-1} is due to the O–H stretching of residual adsorbed water, which is about 30% lower in the aged sample. The lower content of adsorbed water may be also responsible for the lower absorption in the O–H bending region (around 1642 cm^{-1}). The absorptions of polyacrylate are observed as a convolution of peaks at 1555 and 1409 cm^{-1}; vinyl binder and
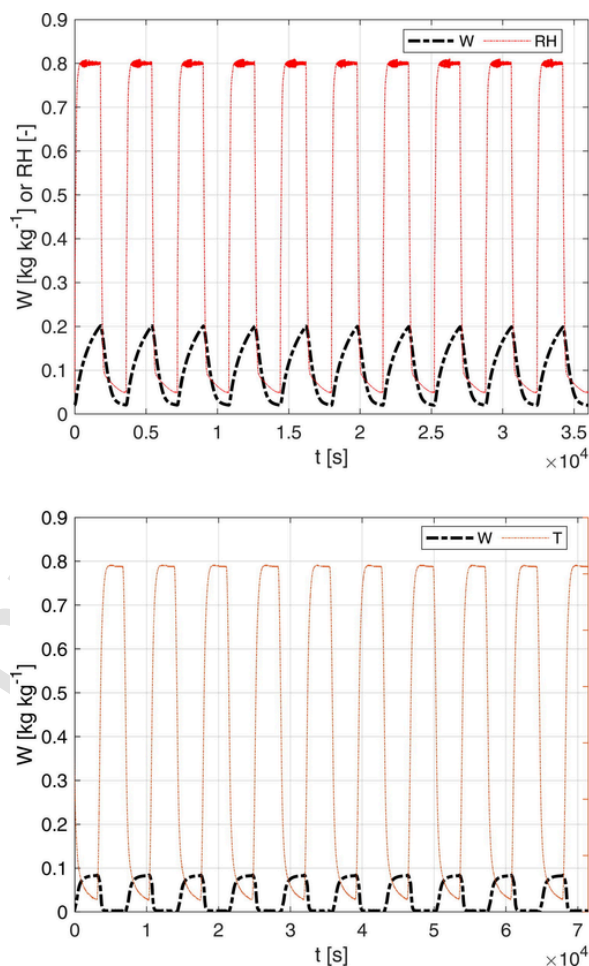

Fig. 8. Water content and relative humidity or temperature profile during stability cycles in DVS: constant temperature and variable relative humidity (top) and both variable temperature and relative humidity (bottom).

polypropylene absorption are present at 1729, 1452 and 699 cm^{-1}. The main absorption band between 1300 and 800 cm^{-1} is due to silica. The absorptions at 1052 and 794 cm^{-1} are due to the Si-O asymmetric and symmetric stretching, respectively. The shoulder at 962 cm^{-1} is due to the C-O Si-O-C bending.

The vibrational analysis did not show any significant variation of the material except for a decrease of the polyacrylate peak at 1555 cm^{-1} and for the shoulder at 962 cm^{-1}, in the silica absorption region. Considering that sodium polyacrylate is soluble in water, we could suggest that ageing may induce its slight dissolution because of hydrogen bonding interactions between the water and the polymer [44].

The decrease of the shoulder at 962 cm^{-1} in the silica absorption region may be due to a slow degradation of silica network due to ageing. For this reason, the 1300–800 cm^{-1} region of FTIR spectra of solid silica gels was further investigated through the peak fitting analysis [45]. This region is indeed the convolution of several bands [46] and the identification of the single components may give structural information about silica solutions and the potential occurrence of the sol–gel process [41–45]. Fig. 9B shows the results of the peak fitting analysis of the 1350–870 cm^{-1} region of ATR-FTIR spectra of virgin and aged material and Fig. 9C shows the optical density (OD) percentage of each component resulting from the peak fitting (N = 3 replicates). The mean standard error between the experimental and the theoretical curves was in all cases < 5 × 10^{-6}.
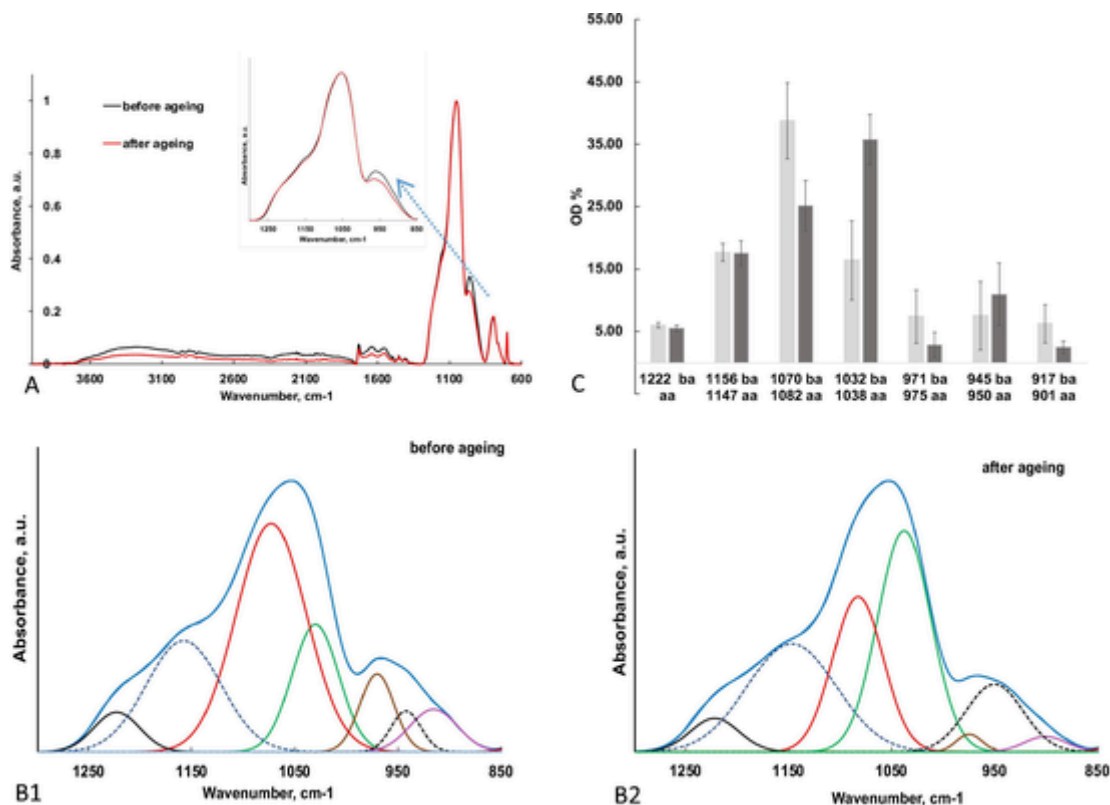
Fig. 9. (A) Normalized FT-IR spectra of the material before (black line) and after (red line) ageing. (B) Peak fitting analysis of 1350–870 cm^{-1} region of ATR-FTIR spectra of virgin (B1) and aged material (B2); the peak fitting was performed with 7 gaussian peaks [45]. The spectrum deconvolution software identified 7 Gaussian peaks: around 1222 cm^{-1} (black continuous line), around 1156–1147 cm^{-1} (blue dotted line), 1070–1082 cm^{-1} (red line), 1032–1038 cm^{-1} (green line), 971–975 cm^{-1} (brown line), 945–950 cm^{-1} (black dotted line) and 917–901 cm^{-1} (purple line); the assignment of each single component is reported in the text. (C) optical density (OD) percentage of each component resulting from the peak fitting (N = 3 replicates); ba = before ageing (light gray columns) and a = after ageing (dark gray columns). ATR-FTIR spectra have been normalized with respect to the highest peak in the 1350–870 cm^{-1} region. (For interpretation of the references to colour in this figure legend, the reader is referred to the web version of this article.)

A deep inspection of this region evidence indeed changes in the silica network that, however, do not have a big impact on the performances of the material developed in this study.

In this region, characteristic peaks identified also by Osswald et al. [46] are observed around 1222, 1156–1147, 1070–1082, 1032–1038, 971–975, 945–950 and 917–901 cm^{-1}. The frequency and the OD % of most of them changes with ageing. The first absorption at 1222 cm^{-1} is assigned to the LO$_3$ mode of Si-O-Si asymmetric stretching vibration [48]. The shoulder at 1167–1147 cm^{-1} may be due to skeletal Si-O stretching vibrations [49 50] or to the LO$_3$ mode of the Si–O–Si stretching vibration in porous gel silica [47 48]. The peak around 1070–1082 cm^{-1} has been assigned to the TO$_3$ mode of Si—O—Si asymmetric stretching vibration [46 47 49–51]. The additional peak at 1032–1038 cm^{-1} has been assigned to TO$_3$ mode of surface Si-O-Si stretching, while for inner Si—O—Si the same absorption is at 1098–1074 cm^{-1} [46]. After ageing the contribution to the main peak of silica network is due to surface Si—O—Si stretching that suggests a degradation of silica network. The peak around 1038 cm^{-1} has high intensity when particle size is small and, therefore, the surface/volume ratio is high [46]. For bigger particles the asymmetric Si—O—Si stretching mode at ∼ 1080–1100 cm^{-1} is dominant.

After ageing the shoulder around 962 cm^{-1} is mainly due to the component at 950 cm^{-1} assigned to the stretching vibration of Si—O of silanol groups [52], likely formed after many sorption/desorption cycles.

3.3.2. Thermal stability

Fig. 10 shows the TGA curve (solid line) obtained for a sample of a desiccant sheet. Two different weight drops can be identified at low
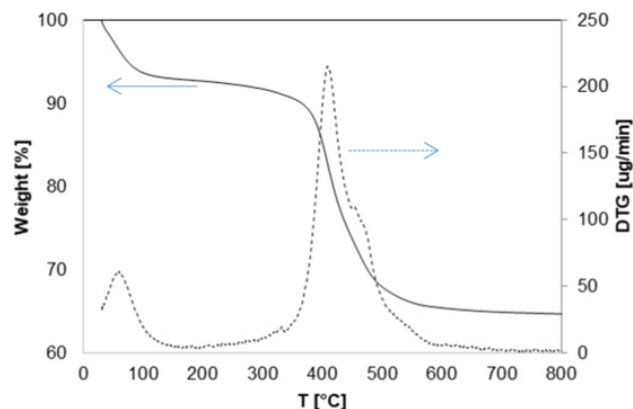

Fig. 10. TG (solid line) and DTG (dotted line) profile of the desiccant sheet. Maximum rate of weight loss at 60 °C and 410 °C.

and high temperature. *i)* At about 60 °C a first weight loss of ∼ 6% can be identified. It is attributed to the evaporation of the water vapor adsorbed by the silica gel from the humid air. This weight drop at low temperature could be also supported by the additional evaporation of the residual organic solvents not released during the drying phase in oven at 75 °C. *ii)* a second relevant drop in weight (∼20%) was experienced at nearly 400 °C. At this temperature the decomposition of the polymeric binder occurs thus setting this temperature as a threshold value for its use. The threshold value of 400 °C is quite higher than the typical operating conditions of devices for air humidification and dehumidification (max operating temperature around 100 °C). These re-

sults consequently confirm that the thermal stability of the material is compatible with the application conditions.

To better clarify the nature of the compounds released by the material at low temperatures, HS-GC/MS analysis was applied to evaluate the release of volatile and potentially harmful compounds following the heating of the desiccant sheet [45]. Samples of desiccant sheet (1 g, corresponding to 25 cm²) were analyzed before and after thermal annealing at 80 °C under vacuum for 8 h.

The headspace above the desiccant sheet, closed into a gas-tight vial, was injected into a GC–MS instrument after mild heating at 80 °C for 15 min, and the analysis was repeated three times on the same sample. Several organic compounds were identified from their mass spectra, and the intensity of each signal (expressed as detector counts) was compared among the three analyses. Specifically, the headspace analysis of the desiccant sheet before 8-hours thermal annealing showed the presence of organic solvents such as acetone, 2-propanol, and ethanol (Fig. 11). Traces of organic solvents can be found in glue or in polypropylene as residuals of the peroxide degradation during the industrial manufacturing process, while branched aliphatic hydrocarbons are caused by either polymerization defects or polypropylene thermal degradation at 80 °C [53].

As expected, even a short treatment at 80 °C for 15 min causes the release of volatile compounds from the sample. However, successive analyses on the same desiccant sheet revealed that all compounds were reduced by 80–95% after the first extraction (80 °C for 15 min). This result confirm that the first weight drop in TGA can be ascribed mainly to solvents than water. Moreover, from the analysis of the same sample before and after the thermal annealing for 8 h under vacuum it was possible to observe a significant reduction in the amount of released VOCs (data not shown for brevity). This means that even a mild thermal treatment of the material is sufficient to remove most of volatile organic residues, thus improving its safety and environmental impact.

4. Experimental test of scaled up prototype

4.1. Prototype description and adopted methodology

A small-scale prototype was manufactured in order to evaluate the performance of the proposed composite material. As shown in Fig. 12, the device consists of three rows of desiccant sheets, prepared according to the detailed experimental methodology. Each sheet is 2 mm high, 11.9 cm wide (B_d) and 5.8 cm long (L_d). In each row there are twenty sheets, which are spaced 2 mm apart and are kept in their position through 3D printed plastic supports (the desiccant device height H_d is therefore 7.8 cm). The total dry mass of the sixty sheets is 0.265 kg, which corresponds to a net mass of silica gel M_{SG} equal to 0.193 kg (according to $f_{SG} = 0.73$). The desiccant sheets and related supports are fixed in a Plexiglas box, which is covered with 5 cm tick insulating panels during tests. The cross-sectional area $S = B_d H_d$ of the device is 92.8 cm². Two additional junction ducts were installed to convey the airflow that does not pass through the desiccant sheets during experiments. The box is connected to air ducts of the test rig and mounted on a sliding slide, to allow primary and secondary air flow exchange.

The developed system is compared with a silica gel packed bed device, as reference technology. In particular, the face area S of the system crossed by the airflow and the total mass of desiccant material M_{SG} are set equal to ones of the proposed device (respectively $S = 92.8$ cm² and $M_{SG} = 0.193$ kg). Bed length is calculated as follows:

$$L_{bed} = \frac{M_{SG}}{S \rho_{bed}} \tag{3}$$

In the analysis, experimental data of the developed apparatus are compared with numerical results of the reference one, obtained through a previously developed transient phenomenological model [54]. In such model temperature, humidity ratio and sorbent water content are assumed uniform at the cross section of the bed. In addition, mass transfer resistance through desiccant beads is modelled through an appropriate superficial mass transfer coefficient. The resulting model requires low computation time and guarantees adequate accu-
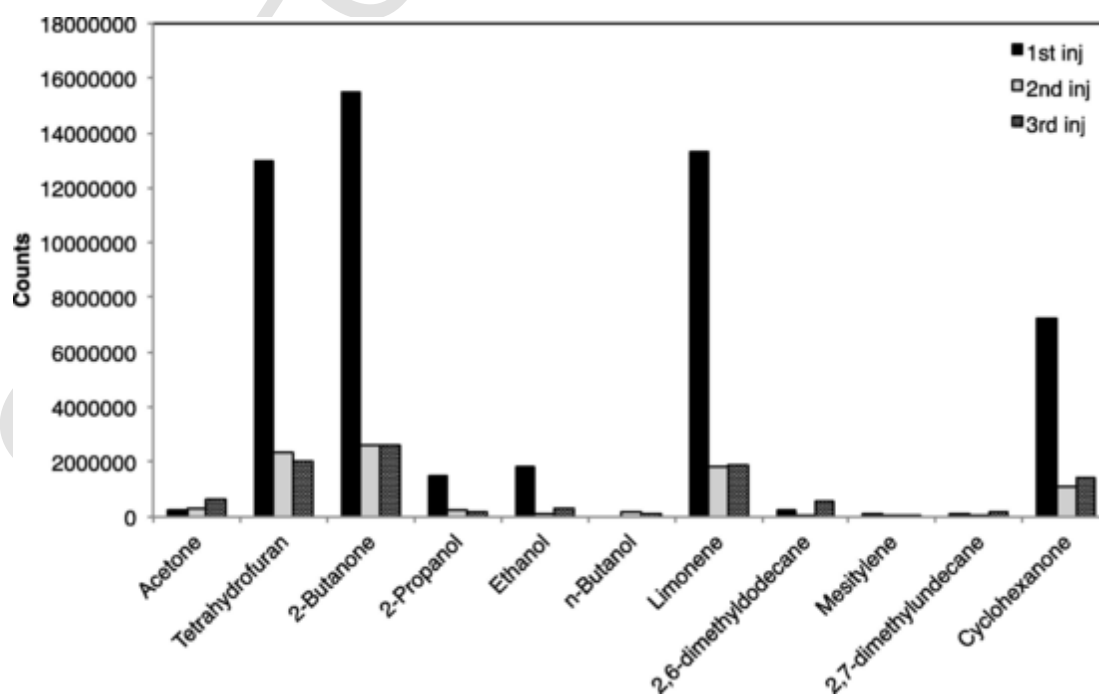

Fig. 11. Chromatographic areas of volatile compounds released from the desiccant sheet before thermal annealing (inj = injection). Before each analysis the sample was heated at 80 °C for 15 min.
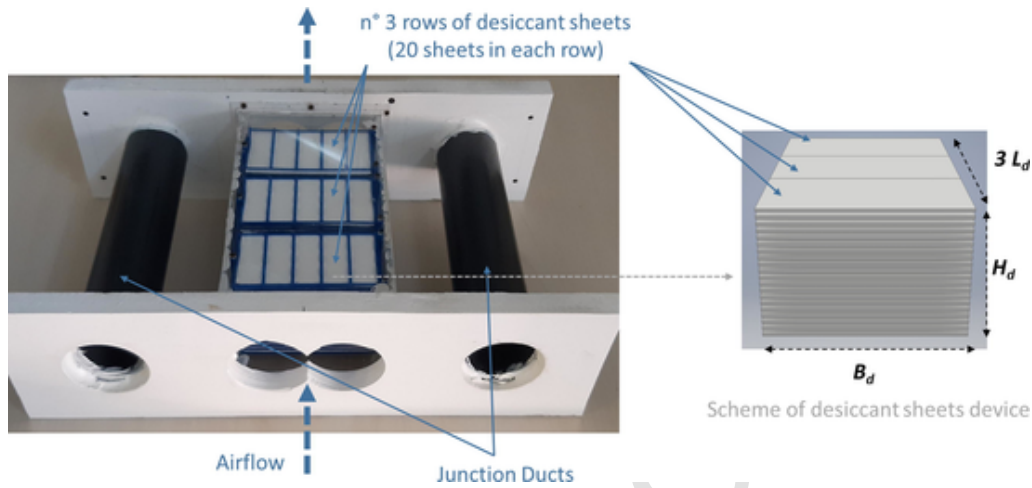
Fig. 12. View of the prototype.

racy of results. Table 3 resumes the main technical data of the packed bed adopted in the simulations.

4.2. Description of the test rig

According to Fig. 13, the test rig consists of two air circuits, namely the process and regeneration one. The desiccant sheets are alternatively connected to the first or second circuit: during the process period (τ_{pro}) the air is dehumidified and heated while during the regeneration step (τ_{reg}) the water is removed from the desiccant material. Inlet process air conditions, namely temperature, relative humidity, and mass flow rate are properly set through two independent air-handling units. The volu-

metric flow rate was evaluated through orifices plates and piezo-resistive pressure sensors ($\pm 0.5\%$ of reading ± 1 Pa), according to DIN EN ISO 5167–2 international standard. Inlet and outlet temperature was measured through calibrated thermocouples (± 0.5 °C) installed in proximity of the desiccant sheet. Airflow humidity ratio was evaluated through coupled PT100 thermo-resistances (± 0.2 °C at 20 °C) and relative humidity capacitive sensors ($\pm 1\%$ at 20 °C) installed in the test rig ducts.

4.3. Experimental results and comparison with reference technology

Experimental tests of the device with the proposed composite materials and numerical simulations of the reference system were carried out in three different operating conditions, summarized in Table 4. Tests were performed with almost the same inlet air conditions (accordingly to experimental setup constraints), representing a dehumidification process with regeneration at low temperature, and three different commutation periods τ. The scope of such tests is to demonstrate that the proposed compound can be used to develop devices for air humidification and dehumidification.

Temperature and humidity ratio profiles of Test A are reported in Fig. 14. It is possible to state that:

i. During the process period, air is dehumidified and heated due to the release of the adsorption heat. The opposite occurs during the regeneration process.
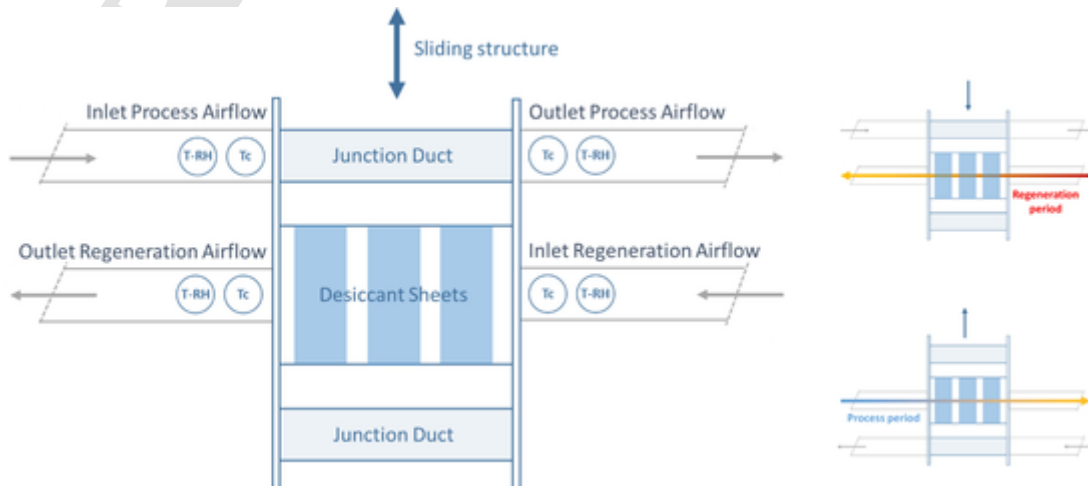
Table 3
Main reference system data adopted in the simulation.

Type of material	Silica Gel
Max water uptake - W_{max} [kg kg^{-1}]	0.318
Average pore size [nm]	2
Water uptake at $T = 50$ °C, $RH = 90$ % – W [kg kg^{-1}]	0.31
Water uptake at $T = 50$ °C, $RH = 40$ % – W [kg kg^{-1}]	0.17
Beads diameter - D_b [mm]	3.3
Packed bed density - ϱ_{bed} [kg m^{-3}]	844
Bed face area - S [cm^2]	92.8
Bed thickness - L_{bed} [cm]	2.5

Fig. 13. Scheme of the experimental setup.

Table 4
Main reference system data adopted in the simulation.

Input

Test	τ [s]	$T_{reg,in}$ [°C]	$X_{reg,in}$ [g kg^{-1}]	$v^N_{reg,in}$ [m s^{-1}]	$T_{pro,in}$ [°C]	$X_{pro,in}$ [g kg^{-1}]	$v^N_{pro,in}$ [m s^{-1}]
A	600	52.1	10.2	0.292	25.4	15.5	0.325
B	1200	52.2	11.1	0.293	24.8	16.1	0.326
C	1800	52.4	10.7	0.293	25.2	16.2	0.327

Output

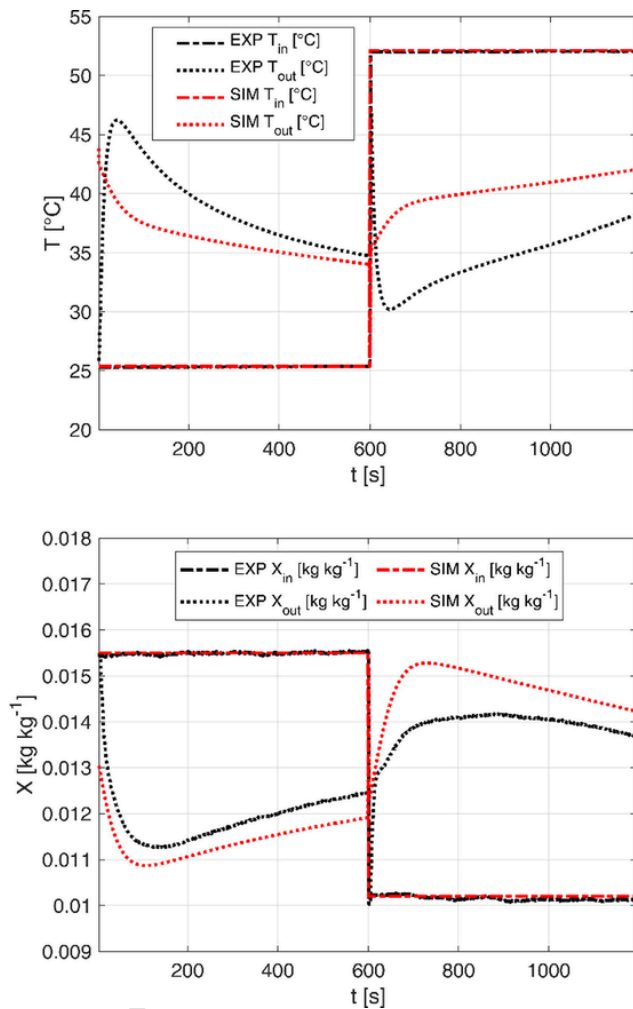|		EXP		SIM		Relative difference	
Test	τ [s]	$\Delta X_{avg,reg}$ [g kg^{-1}]	$\Delta X_{avg,pro}$ [g kg^{-1}]	$\Delta X_{avg,reg}$ [g kg^{-1}]	$\Delta X_{avg,pro}$ [g kg^{-1}]	$\Delta X_{avg,reg}$ [%]	$\Delta X_{avg,pro}$ [%]
A	600	3.8	−3.5	4.5	−4.1	−16%	−13%
B	1200	4.0	−3.4	4.6	−4.1	−14%	−17%
C	1800	3.7	−3.2	4.4	−4.0	−16%	−20%

Fig. 14. Temperature and humidity ratio profile during the entire cycle (process and regeneration period) of Test A.

ii. At the beginning of the process period, the air dehumidification is less effective because the desiccant material is still hot from the regeneration one. Once the structure is adequately cooled, the dehumidification process reaches the maximum value ($t \approx 100$ s) and then it gradually decreases due to the increasing water content in the adsorbent material. A similar analysis can be carried out for the regeneration process.

iii. At the beginning of the commutation period, the experimental temperature difference between outlet and inlet states ($|T_{out}\text{-}T_{in}|$)

is significantly higher than the numerical one obtained for the reference system. This trend is related to the additional thermal capacity of the device (plastic supports, Plexiglas box and ducts) and the consequent transient heat transfer with the airflow. In fact, in the adopted phenomenological model only the thermal capacity of silica gel is considered, leading to a faster desiccant beads cooling/heating after commutation. For this reason, the outlet temperature profile of experiments and simulations are not strictly comparable.

Table 4 reports the time averaged humidity ratio variation ΔX_{avg}, calculated for the process and regeneration period, for both experimental and numerical cases. Dehumidification capacity of the proposed system is always slighter lower than that of the reference technology: the relative difference of $\Delta X_{avg,pro}$ is between 13% and 20%. The difference is mainly related to: *i)* the presence of the glue that partially reduce silica gel interface area and, therefore, adsorption capacity; *ii)* the slightly different properties of silica gel. The preliminary results obtained with this prototype are satisfactory and they can be improved by a further optimization of the device and of operating conditions, such as the regeneration temperature and airflow rates. Furthermore, the proposed system can be designed with different geometries and it does not present the risk of adsorbent grain displacement.

5. Conclusions

In this research a new silica gel-based compound has been proposed for devices aimed at realizing air dehumidification and humidification processes. The proposed formulation is based on a proper combination of silica gel, sodium polyacrylate, vinyl glue and polypropylene fibers. The results of this study have shown that:

(i). The adsorption capacity of the compound at *RH* equal to 90% is 0.32 kg kg^{-1}, highlighting that almost 60% of the silica gel properly works for adsorption/ desorption of water vapor.

(ii). Adequate mechanical strength and high adsorption and thermal stability of on-purpose aged samples were observed.

(iii). The emission of volatile compounds is low and it significantly decreases with progressive thermal cycles. An appropriate pre-treatment of the proposed material, such as vacuum heating, can reduce drastically volatile compounds emissions even after the first cycles.

(iv). Dehumidification capacity of the proposed prototype is around 3.5 g kg^{-1} when the regeneration occurs at 52 °C, slightly lower than that of similar systems based on silica gel beads.

Based on the mentioned results, the silica gel-based compound proposed in this work seems a promising, performing solution that can be used to realize devices for air humidification and dehumidification. Further studies should deal with the design and optimization of the devices, their integration and scale-up in air handling units.

Declaration of Competing Interest

The authors declare that they have no known competing financial interests or personal relationships that could have appeared to influence the work reported in this paper.

References

[1] M. Sahlot, S.B. Riffat, Desiccant cooling systems: a review, Int. J. Low-Carbon Technol. 11 (2016) 489–505, https://doi.org/10.1093/ijlct/ctv032.
[2] O. Labban, T. Chen, A.F. Ghoniem, J.H. Lienhard, L.K. Norford, Next-generation HVAC: prospects for and limitations of desiccant and membrane-based dehumidification and cooling, Appl. Energy. 200 (2017) 330–346, https://doi.org/10.1016/j.apenergy.2017.05.051.
[3] L.H. Zhao, R.Z. Wang, T.S. Ge, Desiccant coated heat exchanger and its

applications, Int. J. Refrig. 130 (2021) 217–232, https://doi.org/10.1016/j.ijrefrig.2021.06.008.

[4] L.W. Wang, R.Z. Wang, R.G. Oliveira, A review on adsorption working pairs for refrigeration, Renew. Sustain. Energy Rev. 13 (2009) 518–534, https://doi.org/10.1016/j.rser.2007.12.002.

[5] W. Wang, L. Wu, Z. Li, Y. Fang, J. Ding, J. Xiao, An overview of adsorbents in the rotary desiccant dehumidifier for air dehumidification, Dry. Technol. 31 (2013) 1334–1345, https://doi.org/10.1080/07373937.2013.792094.

[6] H. Wei Benjamin Teo, A. Chakraborty, W.u. Fan, Improved adsorption characteristics data for AQSOA types zeolites and water systems under static and dynamic conditions, Microporous Mesoporous Mater. 242 (2017) 109–117.

[7] A. Sapienza, G. Gullì, L. Calabrese, V. Palomba, A. Frazzica, V. Brancato, D. La Rosa, S. Vasta, A. Freni, L. Bonaccorsi, G. Cacciola, An innovative adsorptive chiller prototype based on 3 hybrid coated/granular adsorbers, Appl. Energy. 179 (2016) 929–938, https://doi.org/10.1016/j.apenergy.2016.07.056.

[8] L.G. Gordeeva, Y.D. Tu, Q. Pan, M.L. Palash, B.B. Saha, Y.I. Aristov, R.Z. Wang, Metal-organic frameworks for energy conversion and water harvesting: a bridge between thermal engineering and material science, Nano Energy. 84 (2021) 105946, https://doi.org/10.1016/j.nanoen.2021.105946.

[9] A. Karmakar, V. Prabakaran, D. Zhao, K.J. Chua, A review of metal-organic frameworks (MOFs) as energy-efficient desiccants for adsorption driven heat-transformation applications, Appl. Energy. 269 (2020) 115070, https://doi.org/10.1016/j.apenergy.2020.115070.

[10] X. Zheng, T.S. Ge, Y. Jiang, R.Z. Wang, Experimental study on silica gel-LiCl composite desiccants for desiccant coated heat exchanger, Int. J. Refrig. 51 (2015) 24–32, https://doi.org/10.1016/j.ijrefrig.2014.11.015.

[11] M. Djaeni, D.Q. A'yuni, M. Alhanif, C.L. Hii, A.C. Kumoro, Air dehumidification with advance adsorptive materials for food drying: a critical assessment for future prospective, Dry. Technol. 39 (11) (2021) 1648–1666.

[12] K.A. Rocky, A. Pal, T.H. Rupam, M.L. Palash, B.B. Saha, Recent advances of composite adsorbents for heat transformation applications, Therm. Sci. Eng. Prog. 23 (2021) 100900, https://doi.org/10.1016/j.tsep.2021.100900.

[13] Y.I. Aristov, Adsorption dynamics in adsorptive heat transformers: review of new trends, Heat Transf. Eng. 35 (2014) 1014–1027, https://doi.org/10.1080/01457632.2013.863053.

[14] X. Zheng, T.S. Ge, R.Z. Wang, Recent progress on desiccant materials for solid desiccant cooling systems, Energy. 74 (2014) 280–294, https://doi.org/10.1016/j.energy.2014.07.027.

[15] X.N. Wu, T.S. Ge, Y.J. Dai, R.Z. Wang, Review on substrate of solid desiccant dehumidification system, Renew. Sustain. Energy Rev. 82 (2018) 3236–3249, https://doi.org/10.1016/j.rser.2017.10.021.

[16] T. Venegas, M. Qu, K. Nawaz, L. Wang, Critical review and future prospects for desiccant coated heat exchangers: materials, design, and manufacturing, Renew. Sustain. Energy Rev. 151 (2021) 111531, https://doi.org/10.1016/j.rser.2021.111531.

[17] P. Vivekh, M. Kumja, D.T. Bui, K.J. Chua, Recent developments in solid desiccant coated heat exchangers – a review, Appl. Energy. 229 (2018) 778–803, https://doi.org/10.1016/j.apenergy.2018.08.041.

[18] M. Tatlıer, A. Erdem-Şenatalar, The effects of thermal and mass diffusivities on the performance of adsorption heat pumps employing zeolite synthesized on metal supports, Microporous Mesoporous Mater. 28 (1999) 195–203, https://doi.org/10.1016/S1387-1811(98)00301-1.

[19] L. Bonaccorsi, L. Calabrese, A. Freni, E. Proverbio, G. Restuccia, Zeolites direct synthesis on heat exchangers for adsorption heat pumps, in, Appl. Therm. Eng. (2013) 1590–1595, https://doi.org/10.1016/j.applthermaleng.2011.10.028.

[20] L. Bonaccorsi, L. Calabrese, A. Freni, E. Proverbio, Hydrothermal and microwave synthesis of SAPO (CHA) zeolites on aluminium foams for heat pumping applications, Microporous Mesoporous Mater. 167 (2013) 30–37, https://doi.org/10.1016/j.micromeso.2012.06.006.

[21] L. Bonaccorsi, A. Freni, E. Proverbio, G. Restuccia, F. Russo, Zeolite coated copper foams for heat pumping applications, Microporous Mesoporous Mater. 91 (2006) 7–14, https://doi.org/10.1016/j.micromeso.2005.10.045.

[22] L. Bonaccorsi, P. Bruzzaniti, L. Calabrese, A. Freni, E. Proverbio, G. Restuccia, Synthesis of SAPO-34 on graphite foams for adsorber heat exchangers, Appl. Therm. Eng. 61 (2013) 848–852, https://doi.org/10.1016/j.applthermaleng.2013.04.053.

[23] L. Schnabel, M. Tatlier, F. Schmidt, A. Erdem-Senatalar, Adsorption kinetics of zeolite coatings directly crystallized on metal supports for heat pump applications (adsorption kinetics of zeolite coatings), Appl. Therm. Eng. 30 (2010) 1409–1416, https://doi.org/10.1016/j.applthermaleng.2010.02.030.

[24] M.M. Younes, I.I. El-Sharkawy, A.E. Kabeel, K. Uddin, T. Miyazaki, B.B. Saha, Characterization of silica gel-based composites for adsorption cooling applications, Int. J. Refrig. 118 (2020) 345–353, https://doi.org/10.1016/j.ijrefrig.2020.04.002.

[25] B. Dawoud, Water vapor adsorption kinetics on small and full scale zeolite coated adsorbers; a comparison, Appl. Thermal Eng. 50 (2) (2013) 1645–1651.

[26] L. Calabrese, L. Bonaccorsi, A. Freni, E. Proverbio, Silicone composite foams for adsorption heat pump applications, Sustain, Mater. Technol. 12 (2017) 27–34, https://doi.org/10.1016/j.susmat.2017.04.002.

[27] A. Sharafian, K. Fayazmanesh, C. McCague, M. Bahrami, Thermal conductivity and contact resistance of mesoporous silica gel adsorbents bound with polyvinylpyrrolidone in contact with a metallic substrate for adsorption cooling system applications, Int. J. Heat Mass Transf. 79 (2014) 64–71, https://doi.org/10.1016/j.ijheatmasstransfer.2014.07.086.

[28] A. Li, K. Thu, A. Bin Ismail, M.W. Shahzad, K.C. Ng, Performance of adsorbent-embedded heat exchangers using binder-coating method, Int. J. Heat Mass Transf.

[29] 92 (2016) 149–157, https://doi.org/10.1016/j.ijheatmasstransfer.2015.08.097.

[29] P. Vivekh, M.R. Islam, K.J. Chua, Experimental performance evaluation of a composite superabsorbent polymer coated heat exchanger based air dehumidification system, Appl. Energy. 260 (2020) 114256, https://doi.org/10.1016/j.apenergy.2019.114256.

[30] P. Vivekh, D.T. Bui, Y. Wong, M. Kumja, K.J. Chua, Performance evaluation of PVA-LiCl coated heat exchangers for nextgeneration of energy-efficient dehumidification, Appl. Energy. 237 (2019) 733–750, https://doi.org/10.1016/j.apenergy.2019.01.018.

[31] A. Freni, L. Bonaccorsi, L. Calabrese, A. Caprì, A. Frazzica, A. Sapienza, SAPO-34 coated adsorbent heat exchanger for adsorption chillers, Appl. Therm. Eng. 82 (2015) 1–7.

[32] M.M. Younes, I.I. El-sharkawy, A.E. Kabeel, K. Uddin, A. Pal, S. Mitra, K. Thu, B.B. Saha, Synthesis and characterization of silica gel composite with polymer binders for adsorption cooling applications, Int. J. Refrig. 98 (2019) 161–170.

[33] K. Fayazmanesh, et al., Consolidated adsorbent containing graphite flakes for heat-driven water sorption cooling system, Appl. Therm. Eng. 123 (2017) 753–760.

[34] S.J. Oh, K.C. Ng, W. Chun, K.J.E. Chua, Evaluation of a dehumidifier with adsorbent coated heat exchangers for tropical climate operations, Energy 137 (2017) 441–448.

[35] L. Liu, Experimental and theoretical study on water vapor isothermal adsorption-desorption characteristics of desiccant coated adsorber, Int. J. Heat Mass Transf. (2022) 187, 122529.

[36] L.M. Hu, T.S. Ge, Y. Jiang, R.Z. Wang, Performance study on composite desiccant material coated fin-tube heat exchangers Int, J. Heat Mass Transf. 90 (2015) 109–120.

[37] A. Freni, A. Frazzica, B. Dawoud, S. Chmielewski, L. Calabrese, L. Bonaccorsi, Adsorbent coatings for heat pump applications: Verification of hydrothermal and mechanical stabilities, Appl. Thermal Eng. 50 (2) (2013) 1658–1663.

[38] K. Grabowska, J. Krzywanski, W. Nowak, M. Wesolowska, Construction of an innovative adsorbent bed configuration in the adsorption chiller - Selection criteria for effective sorbent-glue pair, Energy. 151 (2018) 317–323, https://doi.org/10.1016/j.energy.2018.03.060.

[39] K. Sztekler, W. Kalawa, A. Mlonka-Medrala, W. Nowak, Ł. Mika, J. Krzywanski, K. Grabowska, M. Sosnowski, M. Debniak, The Effect of Adhesive Additives on Silica Gel Water Sorption Properties, Entropy. 22 (3) (2020) 327.

[40] L. Calabrese, L. Bonaccorsi, A. Caprì, E. Proverbio, Adhesion aspects of hydrophobic silane zeolite coatings for corrosion protection of aluminium substrate, Prog. Org. Coatings. 77 (2014) 1341–1350, https://doi.org/10.1016/j.porgcoat.2014.04.025.

[41] L. Calabrese, L. Bonaccorsi, A. Caprì, E. Proverbio, Electrochemical behavior of hydrophobic silane–zeolite coatings for corrosion protection of aluminum substrate, J. Coatings. Technol. Res. 11 (2014) 883–898, https://doi.org/10.1007/s11998-014-9597-4.

[42] L. Calabrese, L. Bonaccorsi, P. Bruzzaniti, E. Proverbio, A. Freni, SAPO-34 based zeolite coatings for adsorption heat pumps, Energy. 187 (2019) 115981.

[43] A. Frazzica, L.F. Cabeza, eds., Recent Advancements in Materials and Systems for Thermal Energy Storage, Springer International Publishing, Cham, 2019. https://doi.org/10.1007/978-3-319-96640-3.

[44] T. Wang, W. Kang, H. Yang, Z. Li, H. Fan, W. Zheng, T. Zhu, S. Aidarova, M. Gabdullin, Water-soluble grafted sodium polyacrylate with low concentration: Synthesis and thermal properties, J. Mol. Liq. 345 (2022) 117837, https://doi.org/10.1016/j.molliq.2021.117837.

[45] E. Bramanti, M. Bramanti, P. Stiavetti, E. Benedetti, A frequency deconvolution procedure using a conjugate gradient minimization method with suitable constraints, J. Chemom. 8 (1994) 409–421, https://doi.org/10.1002/cem.1180080606.

[46] J. Osswald, K.T. Fehr, FTIR spectroscopic study on liquid silica solutions and nanoscale particle size determination, J. Mater. Sci. 41 (2006) 1335–1339, https://doi.org/10.1007/s10853-006-7327-8.

[47] S. Ponton, F. Dhainaut, H. Vergnes, D. Samelor, D. Sadowski, V. Rouessac, H. Lecoq, T. Sauvage, B. Caussat, C. Vahlas, Investigation of the densification mechanisms and corrosion resistance of amorphous silica films, J. Non. Cryst. Solids. 515 (2019) 34–41, https://doi.org/10.1016/j.jnoncrysol.2019.04.005.

[48] J. Gallardo, A. Durán, D. Di Martino, R.M. Almeida, Structure of inorganic and hybrid SiO2 sol–gel coatings studied by variable incidence infrared spectroscopy, J. Non. Cryst. Solids. 298 (2002) 219–225, https://doi.org/10.1016/S0022-3093(02)00921-3.

[49] M. Muroya, Correlation between the formation of silica skeleton structure and Fourier transform reflection infrared absorption spectroscopy spectra, Colloids Surfaces A Physicochem. Eng. Asp. 157 (1999) 147–155, https://doi.org/10.1016/S0927-7757(99)00054-0.

[50] T.A. Guiton, C.G. Pantano, Infrared reflectance spectroscopy of porous silicas, Colloids Surfaces A Physicochem. Eng. Asp. 74 (1993) 33–46, https://doi.org/10.1016/0927-7757(93)80396-V.

[51] P. Innocenzi, Infrared spectroscopy of sol–gel derived silica-based films: a spectra-microstructure overview, J. Non. Cryst. Solids. 316 (2003) 309–319, https://doi.org/10.1016/S0022-3093(02)01637-X.

[52] M. Hino, T. Sato, Infrared Absorption Spectra of Silica Gel-H216O, D216O, and H218O Systems, Bull. Chem. Soc. Jpn. 44 (1971) 33–37, https://doi.org/10.1246/bcsj.44.33.

[53] C. Badji, J. Beigbeder, H. Garay, A. Bergeret, J.-C. Bénézet, V. Desauziers, Under glass weathering of hemp fibers reinforced polypropylene biocomposites: Impact of Volatile Organic Compounds emissions on indoor air quality, Polym. Degrad. Stab. 149 (2018) 85–95, https://doi.org/10.1016/j.polymdegradstab.2018.01.020.

[54] S. De Antonellis, L. Colombo, A. Freni, C. Joppolo, Feasibility study of a desiccant

packed bed system for air humidification, Energy. 214 (2021) 119002, https://doi.org/10.1016/j.energy.2020.119002.